Effect of wind speed distribution and site assessment on pitch bearing loads and life

Effect of wind speed distribution and site assessment on pitch bearing loads and life

Ashkan Rezaei, Amir R. Nejad

Department of Marine Technology, Norwegian University of Science and Technology (NTNU), NO-7491, Trondheim, Norway

E-mail: ashkan.rezaei@ntnu.no

Abstract. In this paper, the wind speed distribution at thirteen onshore and offshore wind sites has been studied. Different probability distributions are used to estimate the wind speed distribution. Several goodness-of-fit indicators were used to assess the suitability of the fitting. The highest results were achieved by Kernel distribution in both onshore and offshore wind sites. Onshore wind sites did not fit well compared to offshore wind sites. Rayleigh distribution results at onshore wind sites were worse than at offshore wind sites. Onshore and offshore wind distributions result in various load duration distributions in pitch bearing. The concept of life ratio was introduced to compare the long-term fatigue life of the pitch bearing in different wind speed conditions. It is observed that the fatigue life of the pitch bearings in some wind sites is less than that of related IEC classes, and the risk of failure of the pitch bearing before the end of its expected designed fatigue life exists.

1. Introduction

The wind speed distribution at the site is significant for the wind turbine design because it determines the frequency of occurrence of the individual load components.

In wind energy, many distributions are investigated. Carta et al. [1] studied several probability distribution functions (PDFs) using Canary Island case studies. They investigated various PDFs that had one to three parameters. Despite the fact that the Weibull distribution has advantages over the PDFs under study, it is limited in its ability to capture some of the wind regimes that are common in nature, such as those with substantial proportions of null wind speeds, bimodal distributions, etc. For five wind sites in the east and south-east of Iran, Alavi et al. [2] assessed eight different PDFs. Due to its greater fit at two stations, their analysis demonstrated the Nakagami distribution's effectiveness. Jung et al. [3] reviewed 46 studies published between 2010 and 2018, which compared the goodness-of-fit of different theoretical parametric distributions and were evaluated. It was found that the two-parameter Weibull distribution is by far the most frequently evaluated distribution (in 44 out of 46 studies). Shi et al. [4] reviewed different distributions for wind energy. Additionally to investigate at the single and combination wind speed distributions, they also examined non-parametric distribution models including kernel density estimation and the maximum entropy principle. Ahsan-ul-Haq et al. [5] introduced a new three-parameter probability distribution called "New Alpha Power Transformed Power Lindley Distribution (NAPTPL)". They studied the distribution for five district regions of Pakistan and justified that the NAPTPL distribution has favorable performance for all five regions.

In this study, different offshore and onshore wind fields were studied, and the most suitable wind distribution was fitted to the data to compare the results with standard proposed distributions. According to the standards [6, 7], the Rayleigh distribution shall be taken into account for the load calculations for the standard wind turbine classes. However, it does not truly represent wind distribution at wind sites, and according to results, the Rayleigh distribution underestimates the above-rated wind speed at the onshore site while overestimating it at the offshore site. The uncertainty in the wind speed distribution is studied, and the resulting uncertainty in long-term fatigue life is stated.

Besides the wind speed distribution, the wind sites are studied based on wind energy potential [8, 9]. In this work, the wind sites are based on the loads on the blade's root, which is very important for pitch bearing. The pitch bearing is a component that transfers the loads from the blades to the hub and nacelle. The pitch system is the most critical subassembly in offshore and the fourth critical subassembly in onshore sites based on failure rate and downtime [10]. Failure in the pitch bearing consists of fatigue and wear modes [11]. Fatigue mode is categorized into rolling contact fatigue, core crushing, edge loading, and ring fracture. In this paper, rolling contact fatigue is studied, and hereafter, whenever bearing life is mentioned, it refers to rolling contact fatigue. The bearing fatigue life calculation is documented in the National Renewable Energy Laboratory design guideline (DG03) [12]. Despite the existence of other work done by Woll et al. [13] or Breslau et al. [14] to calculate the slewing bearing fatigue life, the DG03 calculation process is referred in standards [15]. A wind turbine and its components are designed based on standards, such as IEC 61400 [7]. These standards are also used to classify wind sites, and wind turbine manufacturers assign wind turbines based on wind site classifications. The life behavior of wind turbine components at real wind sites has not been investigated extensively. This paper presents a study of pitch bearing loads and life in IEC-designed cases and a comparison with real wind site data.

The rest of the paper is organized as follows: Section 2 describes the methodology for wind distribution and load calculations. Wind speed data is given in Section 3. The wind speed and load analysis and its results are presented in Section 4. Finally, Section 5 presented the conclusions.

2. Methodology

The study starts with the different probability distribution functions of wind sites. The wind speeds are projected at different heights. By using the statistical approach, the goodness-of-fit of each distribution function is evaluated, and the result is validated with known data at specific heights.

In the next step, the uncertainty induced on the rotor based on wind speed distribution is compared according to pitch bearing load and life. The main focus is on the blade root loads.

2.1. Wind speed distribution

Different distribution functions are studied. They include generalized extreme value, Gamma, inverse Gaussian, Kernel, lognormal, Nakagami, Rayleigh, Rician, and Weibull. In Table 1, PDFs of the nominated distribution function are presented. More information on the equations and parameters definitions of generalized extreme value, Gamma, Kernel, and Weibull is referred to [4]. The parameters of inverse Gaussian, lognormal, and Nakagami are referred to [2]. Rayleigh and Rician parameters are referred to [16].

Table 1: PDFs of nominated distribution function [2, 4, 16]

Distribution function	PDF
Generalized Extreme Value(GEV)	$f(x) = \frac{1}{\alpha}[1 - \frac{k}{\alpha}(x-\mu)]^{\frac{1}{k}-1} - e^{-[1-\frac{k}{\alpha}(x-\mu)]^{\frac{1}{k}}}$
Gamma(Gam)	$f(x) = \frac{\alpha^k}{\Gamma(k)} x^{k-1} e^{-\alpha x}$
Inverse Gaussian (IG)	$f(x) = \sqrt{\frac{\lambda}{2\pi x^3}} e^{-\frac{\lambda}{2\mu^2 x}(x-\mu^2)}$
Kernel (Ker)	$f(\alpha) = \frac{1}{nh}\sum_{i=1}^{n} K(\alpha), \quad \alpha = \frac{x-x_i}{h}$
Lognormal (LN)	$f(x) = \frac{1}{x\sigma\sqrt{2\pi}} e^{-\frac{1}{2}[\frac{ln(x)-\mu}{\sigma}]^2}$
Nakagami (Nak)	$f(x) = \frac{2m^m}{\Gamma(m)\Omega^m} x^{2m-1} e^{-\frac{m}{\Omega}x^2}$
Rayleigh (Ray)	$f(x) = \frac{x}{\sigma^2} e^{-\frac{x^2}{2\sigma^2}}$
Rician (Ric)	$f(x) = \frac{x}{a^2} e^{-\frac{x^2+b^2}{2a^2}} I_0(\frac{bx}{a^2})$
Weibull (Wbl)	$f(x) = \frac{k}{\alpha}(\frac{x}{\alpha})^{k-1} e^{-(\frac{x}{\alpha})^k}$

In this study, the parameters were calculated by maximum likelihood estimator [17] using MATLAB software.

There are different statistical approaches to assessing the performance and goodness-of-fit (GoF) of the parameter estimation method [4, 18, 19, 20]. In this study, the following unbounded and bounded indicators have been applied.

- Chi-square error χ^2
- Root mean square error (RMSE)
- Kolmogorov-Smirnov test (K-S)
- Coefficient of efficiency (CE)
- Coefficient of determination (R^2)
- Index of agreement (IA)
- Modified index of agreement (MIA)

The equations related to each indicator are presented in Table 2.

Table 2: Nominated applied goodness-of-fit (GoF) indicators [4, 18, 19, 20]

Goodness-of-fit function	Equation
Chi-square error χ^2	$\chi^2 = \sum \frac{(Q_i - \hat{Q}_i)^2}{\hat{Q}_i}$
Relative root mean square error (RMSE)	$RMSE = \frac{\sqrt{\frac{1}{n}\sum (Q_i - \hat{Q}_i)^2}}{\frac{1}{n}\sum Q_i} 100$
Kolmogorov-Smirnov test (K-S)	$KS = max\|F_i - \hat{F}_i\|$
Coefficient of efficiency (CE)	$CE = 1 - \frac{\sum (Q_i - \hat{Q}_i)^2}{\sum (Q_i - \bar{Q})^2}$
Coefficient of determination (R^2)	$R^2 = [\frac{\sum (Q_i - \bar{Q})(\hat{Q}_i - \tilde{Q})}{\sqrt{\sum (Q_i - \bar{Q})^2 \sum (\hat{Q}_i - \tilde{Q})^2}}]^2$
Index of agreement (IA)	$IA = 1 - \frac{\sum (Q_i - \hat{Q}_i)^2}{\sum (\|\hat{Q}_i - \bar{Q}\| + \|Q_i - \bar{Q}_i\|)^2}$
Modified index of agreement (MIA)	$IA = 1 - \frac{\sum (Q_i - \hat{Q}_i)}{\sum (\|\hat{Q}_i - \bar{Q}\| + \|Q_i - \bar{Q}_i\|)}$
Q_i: Observed data at i-th level	
$\hat{Q}_i$: Estimated data at i-th level	
$\bar{Q}$: Mean of observed data	
$\tilde{Q}$: Mean of estimated data	
F_i: CDF value of observed data at i-th level	
$\hat{F}_i$: CDF value of estimated data at i-th level	

The wind speeds are measured at some finite heights, and they need to be projected to different heights. Two mathematical models have been used to model the vertical profile of wind speed: the logarithmic profile (log law) and power law [21]. The power and log laws are presented as follows, respectively:

$$\frac{U(z)}{U(z_r)} = \left(\frac{z}{z_r}\right)^{\alpha} \tag{1}$$

$$\frac{U(z)}{U(z_r)} = \frac{Ln\frac{z}{z_0}}{Ln\frac{z_r}{z_0}} \tag{2}$$

where wind speed (U) at the projected height (z) is calculated from the reference height (z_r), α is the power exponent, and Z_0 is the surface roughness length. Power law exponent and surface roughness can be calculated from two sets of known wind speed data at different heights. The power law exponent is calculated in two different ways. In the first one, U is the average annual wind speed, while in the second one, the power law exponent in every 10-minutes simulation is calculated and a series of exponents is created. Afterward, polynomials of order 0 to 2 are fitted.

2.2. Wind to bearing life ratio

In order to calculate the blade roots' loads from wind, the National Renewable Energy Laboratory's (NREL's) 5 MW reference wind turbine was considered [22]. The wind turbine model is considered from the reference model in GitHub/OpenFAST [23]. The pitch bearing model is considered from reference [24]. The blade roots' loads are calculated using OpenFAST [25].

The relation between blade roots' loads and pitch bearing life is described further. The equivalent dynamic thrust load (P_{ea}) is a constant centric (uniformly distributed) axial load, under whose influence a rolling bearing would have the same life as it would attain under the

actual load conditions [12]. It can be estimated from

$$P_{ea} = 0.75F_r + F_a + \frac{2.5M}{D_{pw}} \tag{3}$$

where F_r, F_a, and M denote the applied radial, axial, and moment loads, respectively. The pitch diameter of the bearing is denoted by D_{pw} [26]. The moment part of equation 3, $2.5M/D_{pw}$, represents the strongest influence on the basic dynamic axial load rating [27]. The basic rating life, L_{10}, expressed in millions of revolutions, is the rating life associated with 90% reliability and given by the following [12].

$$L_{10} = (\frac{C_{a,osc}}{P_{ea}})^p \tag{4}$$

where $C_{a,osc}$ is the basic dynamic axial load rating for oscillation and p denote-s the life exponent, which equals 3 for ball bearings. The formulation of $C_{a,osc}$ depends on a prorated angle of oscillation, θ , in comparison to the critical angle of oscillation, θ_{crit}.

$$C_{a,osc} = \{ \begin{array}{l} C_a(\frac{180^o}{\theta})^{3/10} Z^{0.033} \text{ for } \theta < \theta_{crit} \\ C_a(\frac{180^o}{\theta})^{1/p} \text{ for } \theta \geq \theta_{crit} \end{array} \tag{5}$$

where C_a is the basic dynamic axial load rating and Z is the number of balls. The prorated angle of oscillation, θ is

$$\theta = \frac{\sum_{k=1}^{K} N_k t_k \theta_k}{\sum_{k=1}^{K} N_k t_k} \tag{6}$$

where K is the number of load cases. Parameters t_k and N_k denote the decimal fraction of time and speed of oscillation, respectively, for the bearing operated under the condition yielding θ_k.

L_{10} life can also be determined in hours of operation, L_{10h} as follows, where rotational speed N is expressed in oscillations per minute (opm).

$$L_{10h} = \frac{10^6 L_{10}}{60N} \tag{7}$$

When $\theta < \theta_{crit}$, the contact stresses of the individual rolling elements do not overlap, and each rolling element has its own discrete stressed volume. These individual stressed volumes then must be combined statistically to calculate the overall capacity and life [12]. In this case, combining equations 3 to 7 results in the following equations:

$$L_{10h} = C(P_{ea})^{-3} \theta^{-0.3} \tag{8}$$

where C is a function of pitch bearing characteristics and is a constant. C is calculated as

$$C = \frac{10^6}{60N} C_a Z^{0.033} 180^{0.3} \tag{9}$$

The equation 8 shows that the bearing life,L_{10h} is a function of P_{ea} and θ. It is also possible to calculate the rating life from equation 10 [15]

$$L_{10} = \frac{\sum q_i}{\sum \frac{q_i}{L_{10i}}} \tag{10}$$

where L_{10} is the combined rating life of the bearing, q_i is the time share on the i-th load level, and L_{10i} is the rating life of the bearing on the i-th load level. It is assumed that the

difference of θ in different sites is not significant. By combining Equations 10 and 8 relation between the life of the bearing with respect to load and time share is derived. Life ratio $Lr_{a,b}$ concept is introduced to compare the life of the bearing in two different wind sites (WSa and WSb) by just knowing the time share of the i-th load level ($P_{ea,i}$) in each wind site. The life ratio, which is the relation between the life of the bearing ($L_{10,WSa}$, $L_{10,WSb}$) in two wind sites (a,b), is calculated as

$$Lr_{a,b} = \frac{L_{10,WSa}}{L_{10,WSb}} = \frac{\sum q_{i,WSb}(P_{ea,i})^3}{\sum q_{i,WSa}(P_{ea,i})^3} \tag{11}$$

where $q_{i,WSa}$ and $q_{i,WSa}$ are the time shares of the i-th load level in wind sites a and b, respectively.

3. Wind speed data

In the present study, 13 wind sites in Iran [28], Pakistan [29], Vietnam [30], Ethiopia [31], Denmark [32], and United State of America [33] were studied. The data includes the mean and standard deviation of 10-min wind speed. In order to account for the wind's seasonal effect, data needs to cover an entire year. Nominated wind sites cover a whole year's measurements. In Table 3, in addition to the year of measurement, the geographical location of the wind sites with their longitude and latitude and the measurement height of the wind speed have been shown. The last wind site in the table, Anholt, is offshore, and the others are onshore wind sites.

Table 3: Geographical location of the selected wind sites

Country	Wind site	Latitude	Longitude	measurement height	year
Iran	Khaf	34°29'10.2"N	60°18'32.1"E	10, 30, 40 (m)	2008
Iran	Mil nader	31°05'11.0"N	61°09'23.0"E	10, 30, 40 (m)	2011
Iran	Shourjeh	36°04'18.3"N	49°26'41.2"E	10, 30, 40 (m)	2009
Iran	Khalkhal Bafrajerd	37°32'23.0"N	48°34'27.0"E	10, 30, 40 (m)	2012
Iran	Moaleman	34°51'57.4"N	54°34'25.1"E	10, 30, 40 (m)	2007
Pakistan	Sujawal	24°30'56.0"N	68°11'19.1"E	40, 60, 80 (m)	2017
Vietnam	Thanh Hai	9°53'43.1"N	106°39'39.6"E	40, 60, 80 (m)	2013
Ethiopia	Aysha	10°49'22.2"N	42°30'12.1"E	40, 60, 80 (m)	2020
Ethiopia	Gode	5°34'42.1"N	43°20'22.3"E	40, 60, 80 (m)	2020
Ethiopia	Kebribeyah	8°58'22.6"N	43°14'58.8"E	40, 60, 80 (m)	2020
Ethiopia	Tuluguled	9°39'07.1"N	42°43'09.6"E	40, 60, 80 (m)	2020
USA	NREL's Flatirons Campus	39°54'38.3"N	105°14'05.3"W	20, 50, 80 (m)	2021
Denmark	Anholt	56°35'44.4"N	11°09'09.8"E	65.6, 85.6, 101.6 (m)	2013

4. Result and discussion

The wind measurement at selected offshore and onshore wind sites was fitted with different PDFs. The results for the selected sites are illustrated in Figure 1.

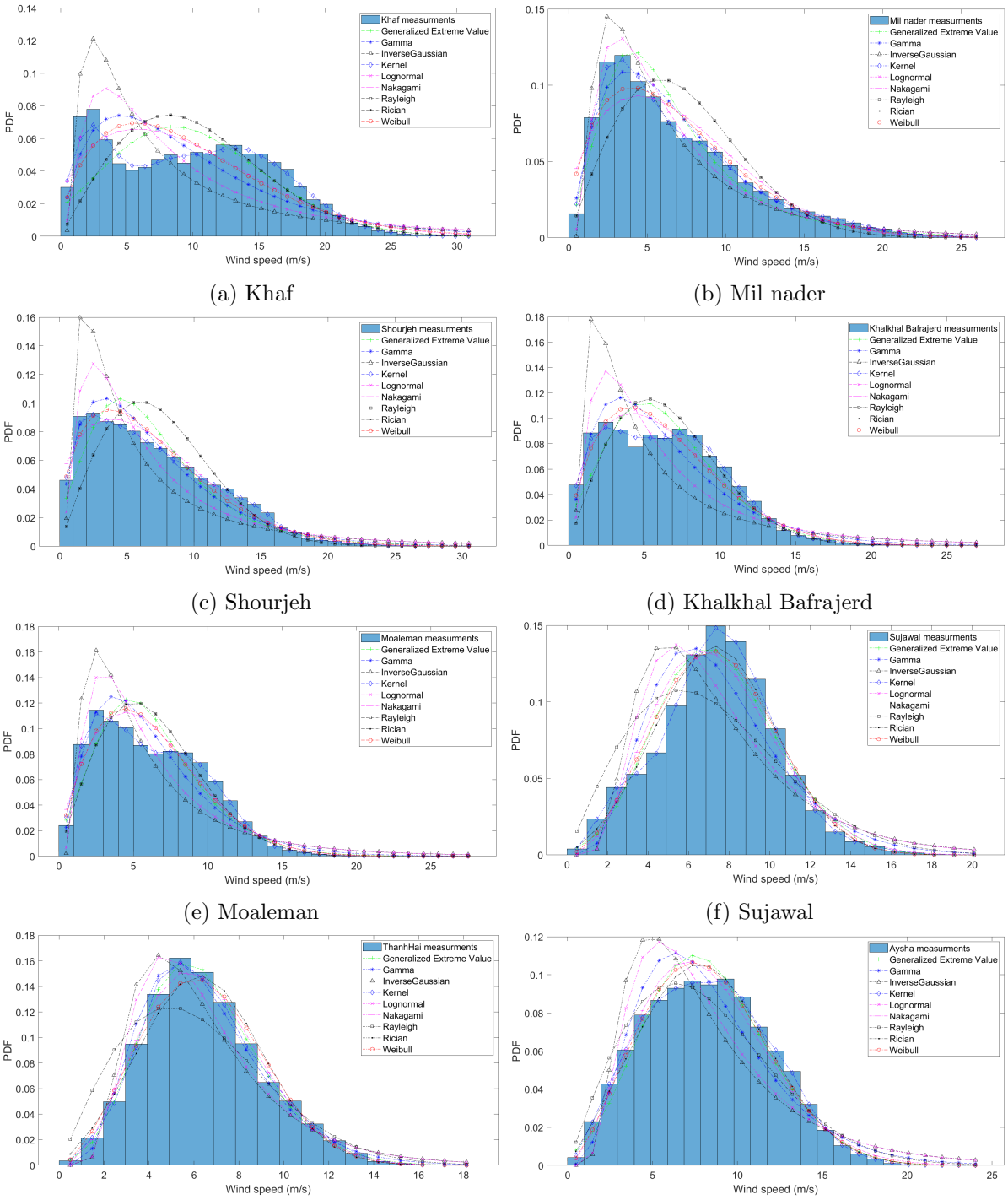

(a) Khaf (b) Mil nader

(c) Shourjeh (d) Khalkhal Bafrajerd

(e) Moaleman (f) Sujawal

(g) ThanhHai (h) Aysha

Figure 1: PDFs of mean wind speed at (a) Khaf, 40m height, (b) Mil nader, 40m height, (c) Shourjeh, 40m height, (d) Khalkhal Bafrajerd, 40m height, (e) Moaleman, 40m height, (f) Sujawal, 80m height, (g) Thanh Hai, 80m height, (h) Aysha, 80m height, (i) Gode, 80m height, (j) Kebribeyah, 80m height, (k) Tuluguled, 80m height, (l) NREL's Flatirons Campus, 80m height, (m) Anholt, 101.6m height

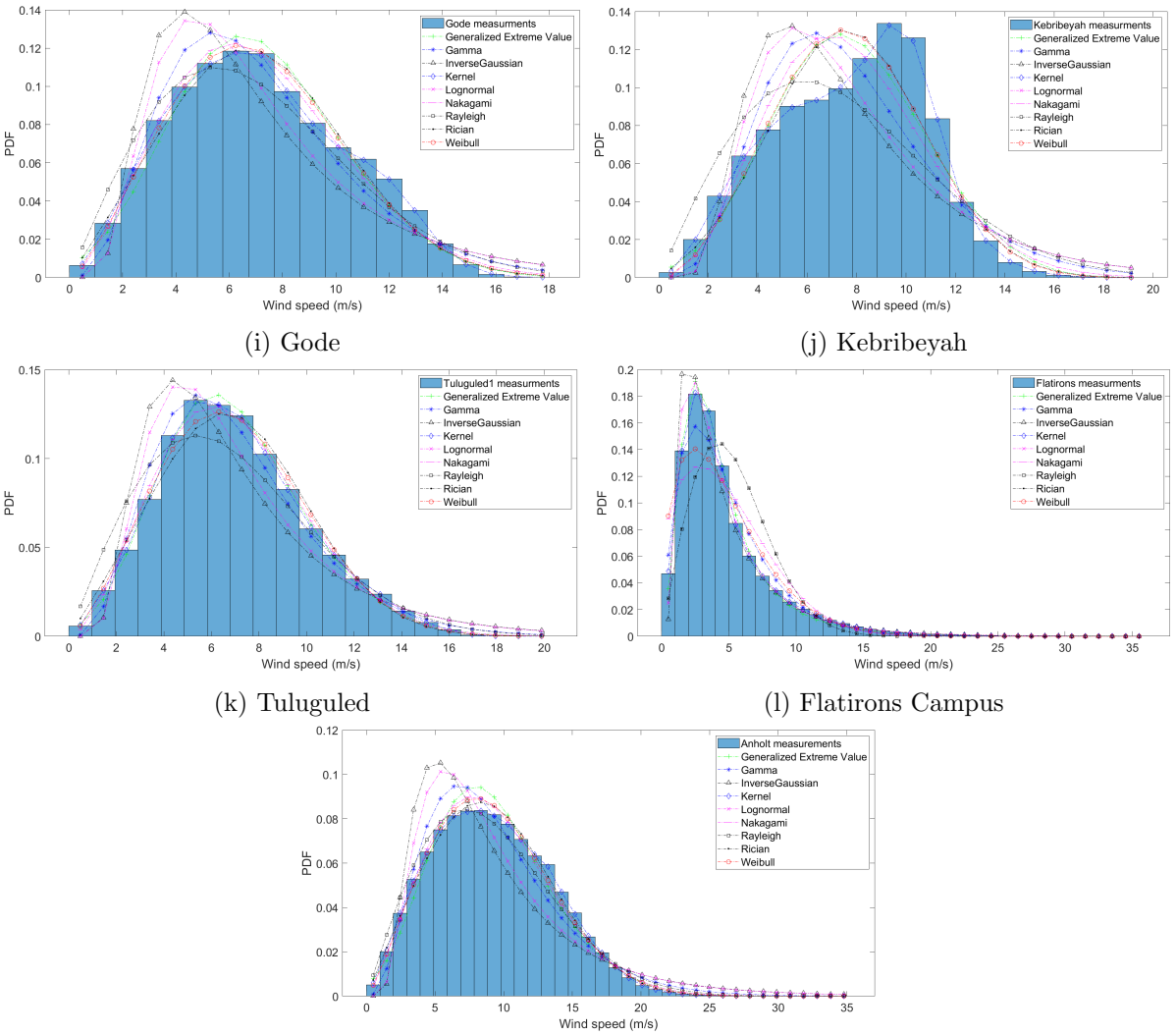

(i) Gode (j) Kebribeyah

(k) Tuluguled (l) Flatirons Campus

(m) Anholt

Figure 1: PDFs of mean wind speed at (a) Khaf, 40m height, (b) Mil nader, 40m height, (c) Shourjeh, 40m height, (d) Khalkhal Bafrajerd, 40m height, (e) Moaleman, 40m height, (f) Sujawal, 80m height, (g) Thanh Hai, 80m height, (h) Aysha, 80m height, (i) Gode, 80m height, (j) Kebribeyah, 80m height, (k) Tuluguled, 80m height, (l) NREL's Flatirons Campus, 80m height, (m) Anholt, 101.6m height

The results show that the Kernel estimator has the best fit. In some sites, such as Khaf or Kebribeyah, Rayleigh distribution, which is proposed by standards and guidelines [6, 7] doesn't fit well. To show how a theoretical probability function matches with the observation data, the results of the considered goodness-of-fit criteria for wind speed data are presented in Table 4 for all selected stations. Generally, the fewer the errors, the better the fit. In χ^2, $RMSE$ and $K-S$ the lower value indicates a distribution better fitted to observation. In CE, R^2, IA and MIA a value close to one indicates better fitting.

Table 4: Goodness-of-fit in different PDFs in selected wind sites

Site	GoF	Distribution functions								
		GEV	Gam	IG	Ker	LN	Nak	Ray	Ric	Wbl
Khaf	χ^2	0.187	0.184	0.716	0.007	0.376	0.111	0.328	0.328	0.143
	RMSE	0.459	0.460	0.722	0.109	0.580	0.379	0.551	0.551	0.430
	K-S	0.095	0.076	0.174	0.040	0.106	0.073	0.151	0.151	0.087
	CE	0.618	0.615	0.052	0.978	0.389	0.739	0.448	0.448	0.664
	R^2	0.658	0.665	0.531	0.980	0.565	0.753	0.583	0.583	0.699
	IA	0.950	0.928	0.861	0.998	0.897	0.954	0.933	0.933	0.942
	MIA	0.775	0.732	0.627	0.951	0.678	0.786	0.742	0.742	0.759
Mil nader	χ^2	0.040	0.018	0.259	0.003	0.048	0.062	0.195	0.195	0.039
	RMSE	0.235	0.161	0.273	0.050	0.178	0.304	0.476	0.476	0.241
	K-S	0.086	0.079	0.051	0.059	0.063	0.097	0.175	0.175	0.081
	CE	0.944	0.974	0.925	0.997	0.968	0.907	0.772	0.771	0.941
	R^2	0.952	0.974	0.955	0.998	0.979	0.908	0.786	0.786	0.942
	IA	0.991	0.996	0.989	1.000	0.994	0.987	0.967	0.967	0.993
	MIA	0.906	0.939	0.893	0.982	0.922	0.886	0.819	0.819	0.917
Shourjeh	χ^2	0.069	0.039	0.280	0.001	0.148	0.015	0.221	0.221	0.021
	RMSE	0.308	0.196	0.653	0.032	0.406	0.147	0.496	0.496	0.156
	K-S	0.080	0.057	0.105	0.042	0.064	0.058	0.160	0.161	0.062
	CE	0.909	0.963	0.588	0.999	0.841	0.979	0.763	0.763	0.977
	R^2	0.919	0.969	0.767	0.999	0.882	0.979	0.809	0.809	0.979
	IA	0.988	0.994	0.947	1.000	0.973	0.997	0.975	0.975	0.997
	MIA	0.889	0.922	0.770	0.990	0.837	0.948	0.841	0.841	0.942
Bafrajerd	χ^2	0.065	0.086	0.419	0.002	0.246	0.028	0.115	0.115	0.041
	RMSE	0.342	0.347	0.789	0.065	0.539	0.225	0.387	0.387	0.269
	K-S	0.086	0.061	0.143	0.048	0.085	0.063	0.126	0.126	0.072
	CE	0.892	0.888	0.422	0.996	0.730	0.953	0.861	0.861	0.933
	R^2	0.901	0.897	0.625	0.996	0.774	0.955	0.887	0.887	0.937
	IA	0.988	0.984	0.925	1.000	0.956	0.994	0.988	0.988	0.992
	MIA	0.891	0.874	0.727	0.981	0.791	0.924	0.893	0.893	0.908
Moaleman	χ^2	0.075	0.068	0.423	0.002	0.199	0.038	0.068	0.068	0.040
	RMSE	0.376	0.303	0.546	0.042	0.431	0.258	0.363	0.363	0.268
	K-S	0.092	0.072	0.073	0.052	0.067	0.076	0.117	0.118	0.077
	CE	0.890	0.929	0.769	0.999	0.856	0.949	0.898	0.898	0.944
	R^2	0.899	0.935	0.827	0.999	0.878	0.950	0.910	0.910	0.947
	IA	0.987	0.990	0.967	1.000	0.978	0.993	0.991	0.991	0.993
	MIA	0.886	0.902	0.818	0.991	0.853	0.919	0.904	0.904	0.915
Sujawal	χ^2	0.040	0.233	> 100	0.001	22.30	0.057	0.175	0.018	0.029
	RMSE	21.16	38.23	61.89	0.799	53.39	26.29	49.79	14.84	18.93
	K-S	0.062	0.061	0.083	0.073	0.083	0.055	0.085	0.065	0.062
	CE	0.958	0.862	0.637	1.000	0.730	0.935	0.765	0.979	0.966
	R^2	0.958	0.862	0.651	1.000	0.735	0.935	0.779	0.979	0.966
	IA	0.993	0.975	0.932	1.000	0.949	0.990	0.944	0.997	0.995
	MIA	0.916	0.842	0.740	0.997	0.775	0.898	0.763	0.943	0.926
Thanh Hai	χ^2	0.004	0.072	> 100	0.002	13.66	0.007	0.107	0.023	0.014
	RMSE	5.197	12.35	33.73	6.013	26.66	8.072	37.58	16.14	13.67
	K-S	0.080	0.056	0.047	0.073	0.045	0.080	0.057	0.099	0.092
	CE	0.997	0.986	0.892	0.997	0.932	0.994	0.866	0.975	0.982

Continuation of Table 4

Site	GoF	Distribution functions								
		GEV	Gam	IG	Ker	LN	Nak	Ray	Ric	Wbl
	R^2	0.998	0.986	0.895	0.997	0.934	0.994	0.884	0.976	0.983
	IA	0.999	0.997	0.980	1.000	0.987	0.999	0.974	0.996	0.997
	MIA	0.978	0.947	0.858	0.980	0.887	0.969	0.839	0.935	0.949
Aysha	χ^2	0.024	0.086	> 100	0.001	2.729	0.019	0.056	0.008	0.010
	RMSE	15.05	25.44	46.85	1.567	39.57	14.32	22.64	9.532	11.19
	K-S	0.063	0.046	0.068	0.048	0.069	0.049	0.043	0.055	0.055
	CE	0.973	0.924	0.741	1.000	0.815	0.976	0.940	0.989	0.985
	R^2	0.976	0.929	0.771	1.000	0.831	0.977	0.943	0.990	0.987
	IA	0.996	0.986	0.955	1.000	0.966	0.996	0.987	0.999	0.998
	MIA	0.936	0.881	0.787	0.994	0.815	0.936	0.888	0.961	0.952
Gode	χ^2	0.028	0.076	> 100	0.001	2.034	0.023	0.050	0.020	0.019
	RMSE	14.55	18.11	37.93	0.797	30.95	10.77	17.69	11.74	10.79
	K-S	0.072	0.050	0.065	0.057	0.065	0.054	0.037	0.067	0.062
	CE	0.963	0.943	0.748	1.000	0.832	0.980	0.945	0.976	0.980
	R^2	0.970	0.951	0.794	1.000	0.859	0.982	0.949	0.977	0.982
	IA	0.992	0.988	0.948	1.000	0.964	0.996	0.986	0.995	0.996
	MIA	0.913	0.891	0.771	0.995	0.811	0.939	0.880	0.933	0.940
Kebribeyah	χ^2	0.072	0.229	> 100	0.001	11.88	0.103	0.213	0.058	0.063
	RMSE	31.67	45.15	60.09	1.248	55.56	36.51	47.19	29.78	30.60
	K-S	0.063	0.073	0.092	0.067	0.094	0.059	0.086	0.065	0.068
	CE	0.879	0.754	0.563	1.000	0.627	0.839	0.731	0.893	0.887
	R^2	0.881	0.762	0.598	1.000	0.649	0.843	0.739	0.896	0.892
	IA	0.981	0.958	0.922	1.000	0.931	0.976	0.943	0.984	0.983
	MIA	0.861	0.795	0.722	0.995	0.737	0.845	0.761	0.874	0.870
Tuluguled	χ^2	0.006	0.067	> 100	0.001	4.435	0.007	0.057	0.015	0.008
	RMSE	5.621	13.95	39.01	1.194	29.74	6.515	26.19	12.84	9.447
	K-S	0.072	0.040	0.050	0.065	0.048	0.064	0.046	0.080	0.073
	CE	0.997	0.979	0.833	1.000	0.903	0.995	0.925	0.982	0.990
	R^2	0.997	0.979	0.843	1.000	0.907	0.995	0.935	0.982	0.990
	IA	0.999	0.996	0.971	1.000	0.981	0.999	0.986	0.997	0.998
	MIA	0.973	0.938	0.829	0.995	0.864	0.970	0.883	0.945	0.959
Flatirons	χ^2	0.012	0.040	0.119	0.001	0.031	> 100	> 100	> 100	0.181
	RMSE	11.12	27.08	44.29	1.504	25.35	58.39	76.77	76.78	46.72
	K-S	0.093	0.112	0.069	0.092	0.078	0.153	0.242	0.242	0.117
	CE	0.996	0.977	0.938	1.000	0.980	0.892	0.813	0.813	0.931
	R^2	0.997	0.978	0.945	1.000	0.981	0.896	0.814	0.814	0.934
	IA	0.999	0.997	0.996	1.000	0.998	0.986	0.976	0.976	0.992
	MIA	0.977	0.947	0.935	0.998	0.960	0.882	0.845	0.845	0.913
Anholt	χ^2	0.037	0.066	> 100	0.001	> 100	0.010	0.023	0.017	0.011
	RMSE	0.160	0.233	0.506	0.013	0.406	0.102	0.151	0.069	0.084
	K-S	0.055	0.040	0.064	0.040	0.062	0.041	0.030	0.046	0.045
	CE	0.979	0.957	0.796	1.000	0.869	0.992	0.982	0.996	0.994
	R^2	0.982	0.959	0.818	1.000	0.878	0.992	0.982	0.996	0.995
	IA	0.997	0.993	0.969	1.000	0.978	0.999	0.997	0.999	0.999
	MIA	0.947	0.917	0.823	0.996	0.853	0.967	0.946	0.977	0.974

The results of unbounded indicators in some distributions increase significantly. In this case, the distribution cannot predict the measurement data, and the value of > 100 is indicated in the table. In addition, the results in the table are rounded, so, for example, a value of 1.000 does not indicate the perfect fitting of the results. From Table 4, ranking wind sites according to different criteria doesn't reach the same result. For example, in Khaf, according to χ^2 indicator, the Weibull distribution fits better with the generalized extreme distribution, while if one considered the CE indicator, the result would be opposite. However, the Kernel has the best goodness of fit results in all wind sites and in all indicators. The result of the proposed Rayleigh distribution is not in the top 3 at any of the wind sites, showing a lack of accuracy in prediction. The results of CE and R^2 have the most consistency with the overall indicators' results. CE distinct results are more significant than R^2. The coefficient of efficiency is considered a present indicator in the rest of the paper.

As stated before, the wind speed at different heights is needed in the study of site assessment. The wind speed data at different heights should be derived artificially from other heights. In order to project data to a specific height, it needs to consider the wind shear. Wind speed projection according to power and log law is performed with different methods. The results of the observed efficiency coefficient and the calculated one by Kernel distribution are presented in Table 5.

Table 5: Coefficient of efficiency in different wind shear at selected wind sites

Site	Distribution function					
	Obs	PMAS	LMAS	PP0	PP1	PP2
Khaf	0.9783	0.9671	0.9672	0.9673	0.9663	0.9717
Mil nader	0.9975	0.9937	0.9941	0.9897	0.9898	0.9897
Shourjeh	0.9990	0.9988	0.9989	0.9990	0.9987	0.9982
Bafrajerd	0.9961	0.9953	0.9953	0.9954	0.9954	0.9957
Moaleman	0.9986	0.9950	0.9943	0.9955	0.9957	0.9954
Sujawal	0.9999	0.9973	0.9962	0.9976	0.9975	0.9982
Thanh Hai	0.9966	0.9976	0.9973	0.9975	0.9974	0.9975
Aysha	0.9997	0.9984	0.9984	0.9983	0.9987	0.9987
Gode	0.9999	0.9852	0.9844	0.9860	0.9887	0.9933
Kebribeyah	0.9998	0.9986	0.9982	0.9984	0.9983	0.9990
Tuluguled	0.9998	0.9992	0.9991	0.9992	0.9992	0.9984
Flatirons	0.9999	0.9971	0.9985	0.9906	0.9843	0.9817
Anholt	0.9999	0.9997	0.9997	0.9997	0.9997	0.9996

Obs: Observation data
PMAS: Power exponent mean annual wind speed
LMAS: Log law mean annual wind speed
PP0: Power exponent polynomial zero degree fitted
PP1: Power exponent polynomial one degree fitted
PP2: Power exponent polynomial two degree fitted

The wind speed at all sites was projected at 90 meters. To project wind speed, a power law with an average power exponent is considered. The calculated power exponent and coefficient of efficiency at 90 meter heights are presented in Table 6.

Table 6: Power law exponent, coefficient of efficiency and mean annual wind speed of projected wind speed to 90 meters height

Wind site	α	CE	Mean annual wind speed(m/s)
Khaf	0.1327	0.8934	10.95
Mil nader	0.1834	0.9455	7.96
Shourjeh	0.0747	0.9895	7.48
Bafrajerd	0.0130	0.9952	6.44
Moaleman	0.2143	0.9164	7.34
Sujawal	0.2102	0.9943	7.62
Thanh Hai	0.2237	0.9947	6.59
Aysha	0.1373	0.9979	8.35
Gode	0.2255	0.9941	7.30
Kebribeyah	0.1450	0.9949	7.86
Tuluguled	0.1725	0.9972	7.10
Anholt	0.1153	0.9993	9.08
Flatirons	0.1248	0.9997	4.81

The wind sites based on their mean annual wind speed at projected height are classified into IEC categories I, II, and III. The PDFs of IEC classes, which use Rayleigh distribution to categorize wind sites, are plotted in Figure 2. Most of the wind sites have been categorized into IEC Classes II and III. In IEC Class I, the offshore site has a higher recurrence at an around-rated wind speed compared to IEC, while the onshore site has a higher recurrence at an over-rated wind speed. In IEC Class II, all sites except Mil Nader have a higher recurrence at the rated wind speed.

The equivalent dynamic load of the pitch bearing in long-term conditions, as well as the wind turbine's life expectancy of 20 years in nominated wind sites and IEC classes, were calculated. Subsequently, the equivalent dynamic loads were distributed into bins to create the load duration distribution (LDD) of the equivalent dynamic loads. LDD shows the contribution of different load levels. The results of the equivalent dynamic load duration distribution in selected wind sites and IEC classes are presented in Figures 3, 4, 5. According to IEC, results are categorized according to annual mean wind speed classes (I, II, and III) and wind speed turbulence (A, B, and C) according to IEC 61400-1 [7]. The results show the contribution of load levels in different wind conditions. In some cases, the contribution of higher equivalent dynamic loads in wind sites exceeds the IECs. It is expected that higher contribution in larger loads will result in a lower life.

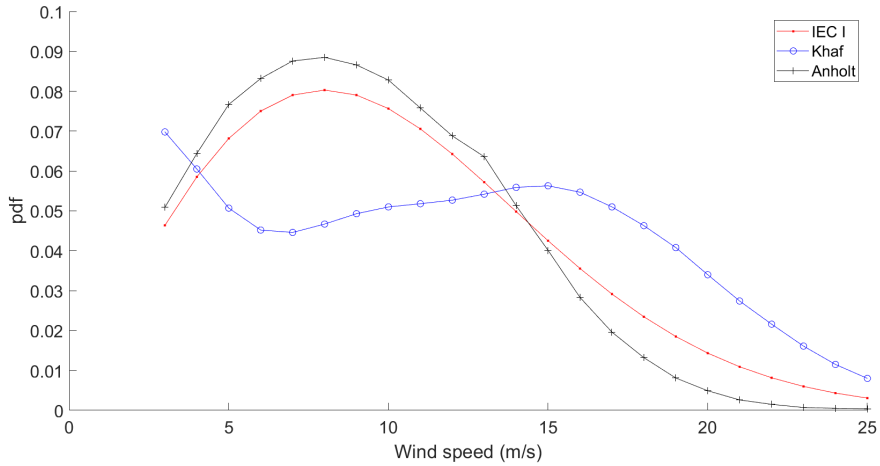

(a) IEC I category

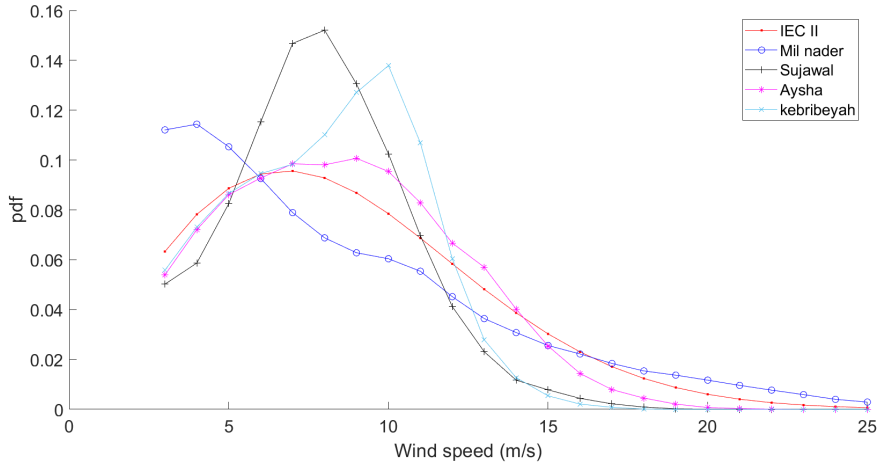

(b) IEC II category

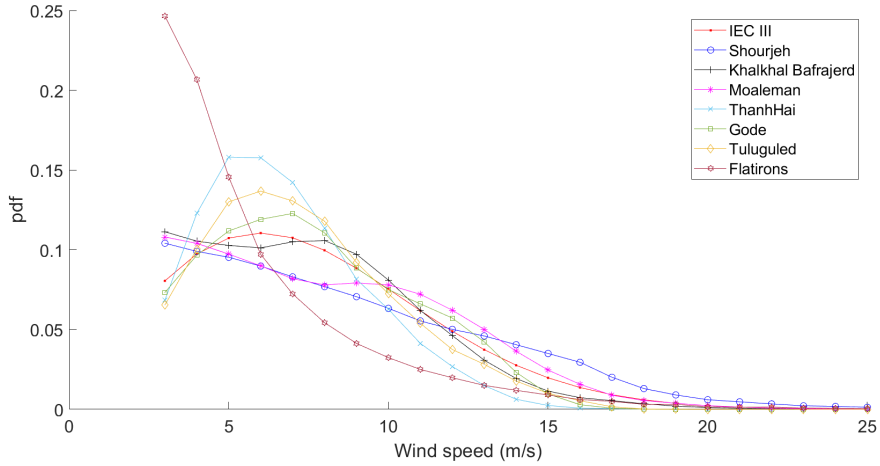

(c) IEC III category

Figure 2: Categorized wind site pdf according to IEC 61400-1 at projected height in category (a) IEC I, (b) IEC II, (c) IEC III

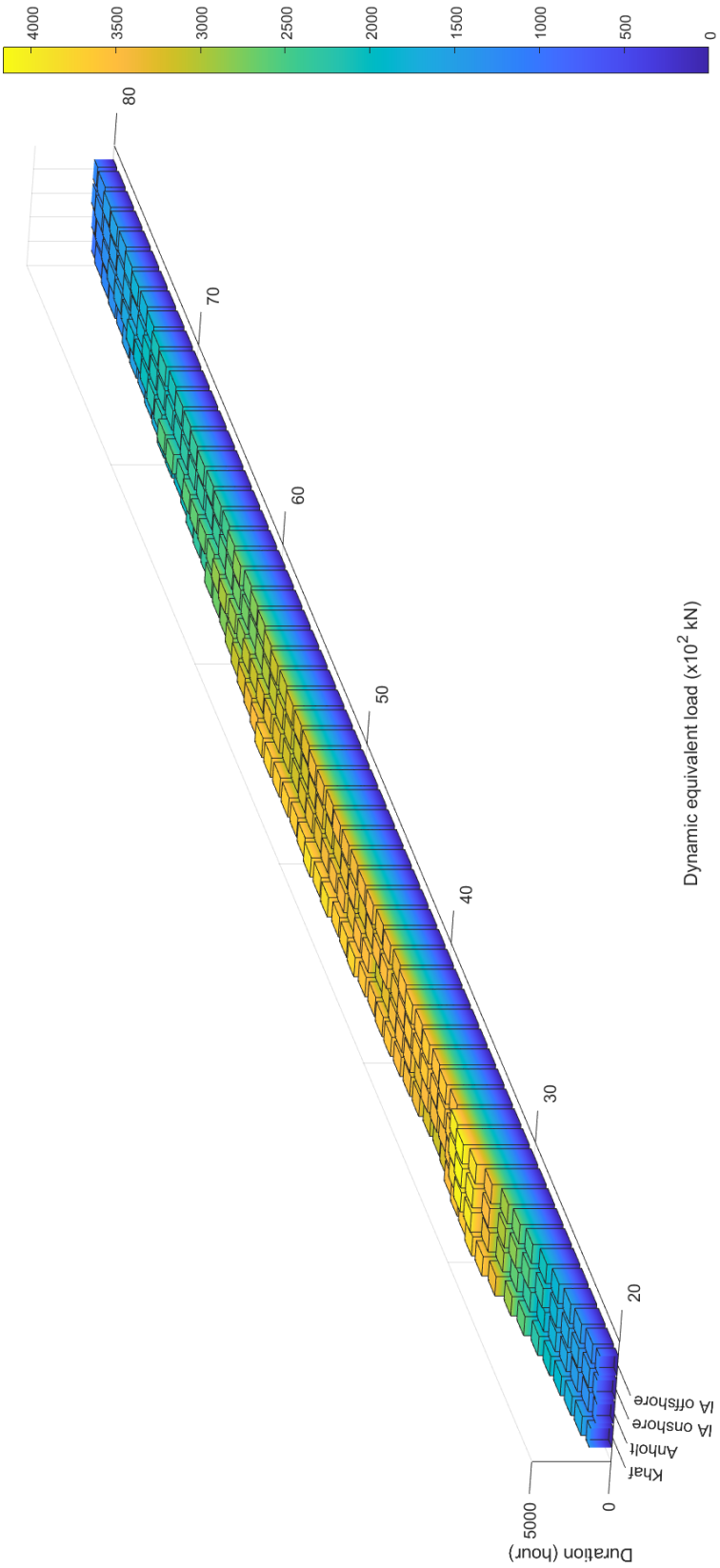

Figure 3: Dynamic equivalent load duration distribution in selected wind sites and IEC class I

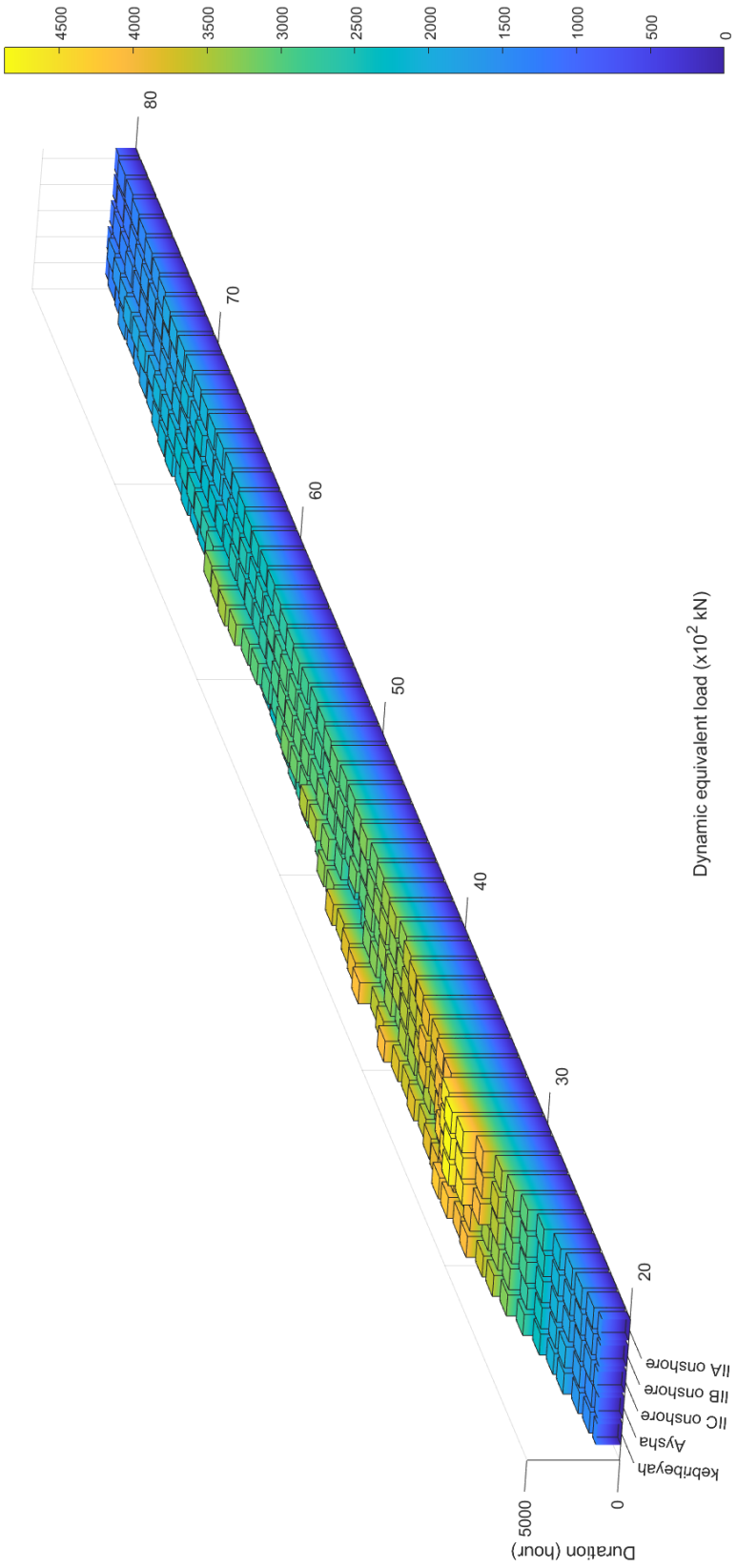

Figure 4: Dynamic equivalent load duration distribution in selected wind sites and IEC class II

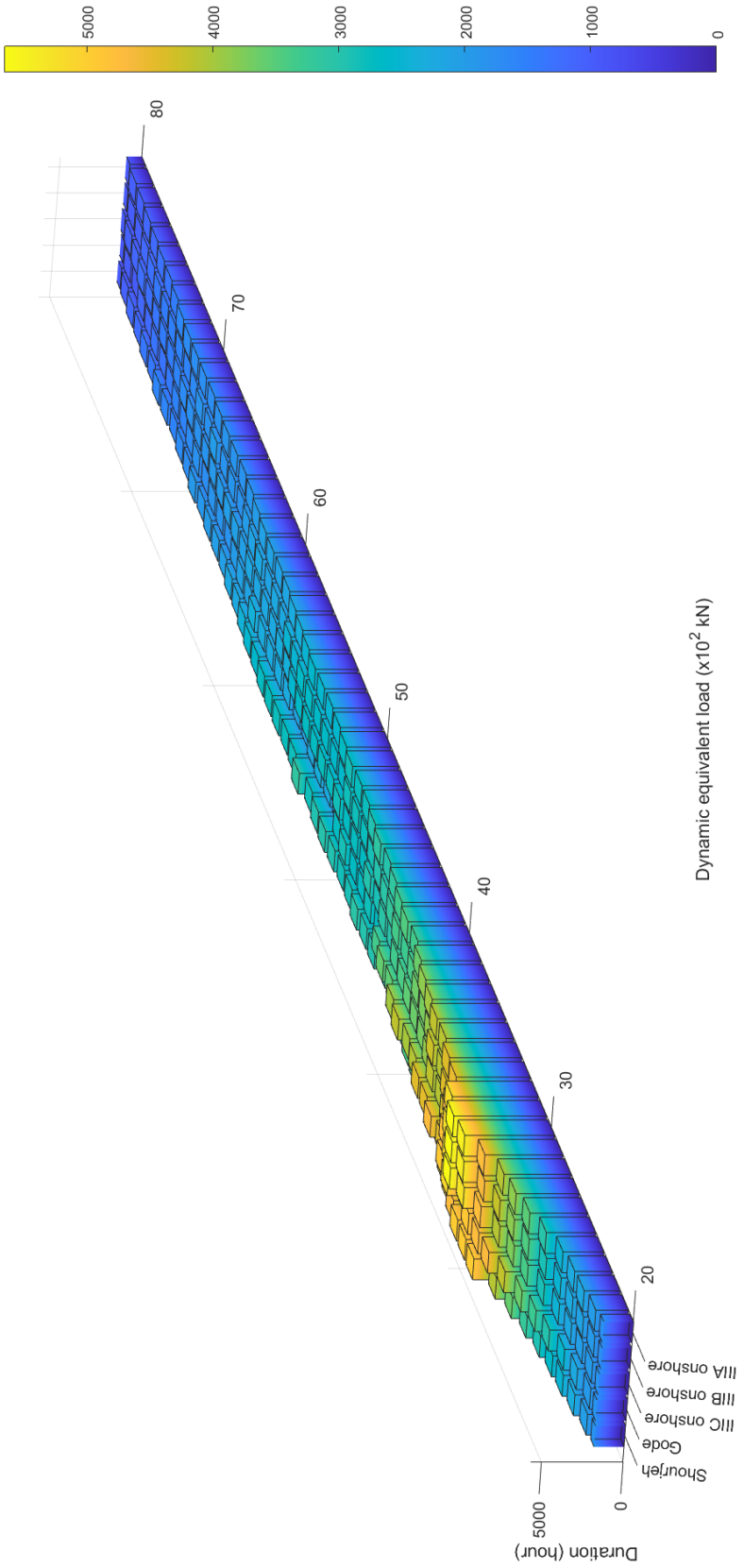

Figure 5: Dynamic equivalent load duration distribution in selected wind sites and IEC class III

In order to compare bearings in different wind sites' conditions, life ratios of bearings in IEC categories with respect to wind sites "$Lr_{IEC,WS}$" are calculated. The life ratio results are presented in Figure 6 and Table 7. The results calculated the life between bearings in IEC categories and nominated wind site conditions. Therefore, the ratio in each bar above one stated that the bearing designed for related IEC conditions is suitable for the mentioned wind site.

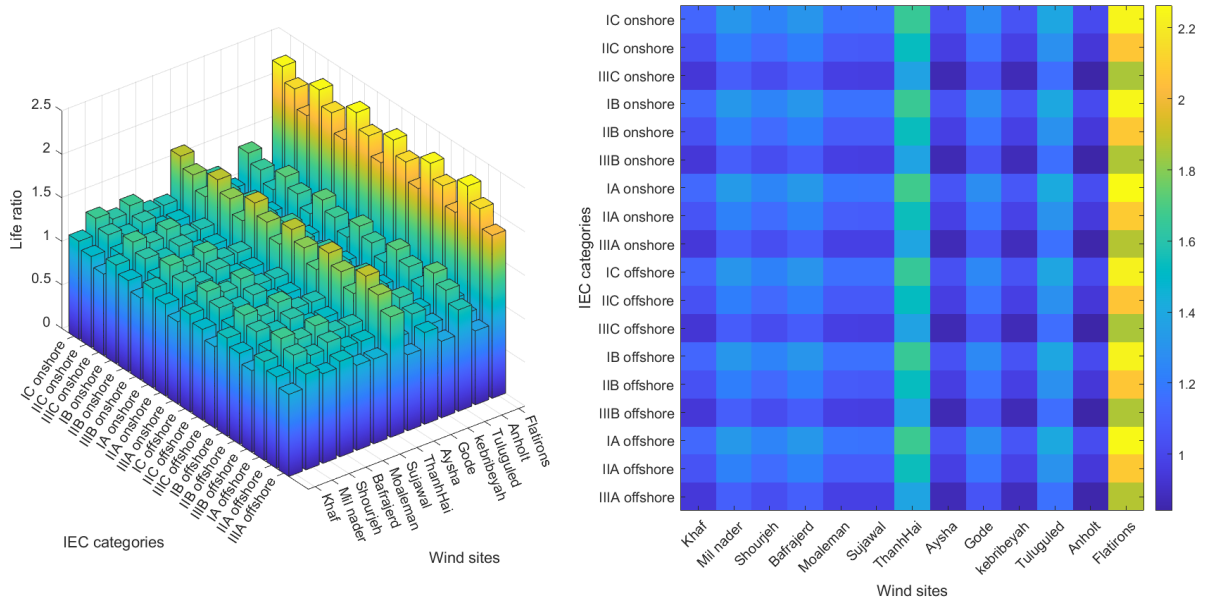

Figure 6: Life ratio factor respect to IEC classes (onshore and offshore) in nominated wind sites

Life ratio (Lr)

IEC categories	Khaf	Mil nader	Shourjeh	Bafrajerd	Moaleman	Sujawal	ThanhHai	Aysha	Gode	kebribeyah	Tuluguled	Flatirons	Anholt
IC onshore	1.13	1.32	1.23	1.31	1.17	1.16	1.66	1.04	1.26	1.05	1.39	2.24	1.01
IIC onshore	1.04	1.22	1.14	1.21	1.08	1.08	1.53	0.97	1.17	0.97	1.29	2.07	0.94
IIIC onshore	0.94	1.09	1.02	1.09	0.97	0.97	1.37	0.87	1.05	0.87	1.16	1.86	0.84
IB onshore	1.13	1.32	1.24	1.32	1.17	1.17	1.66	1.05	1.26	1.06	1.40	2.25	1.02
IIB onshore	1.05	1.22	1.14	1.22	1.08	1.08	1.54	0.97	1.17	0.98	1.29	2.08	0.94
IIIB onshore	0.94	1.09	1.02	1.09	0.97	0.97	1.38	0.87	1.05	0.87	1.16	1.86	0.84
IA onshore	1.14	1.33	1.25	1.33	1.18	1.18	1.67	1.06	1.27	1.06	1.41	2.26	1.03
IIA onshore	1.05	1.23	1.15	1.22	1.09	1.09	1.55	0.97	1.18	0.98	1.30	2.09	0.95
IIIA onshore	0.94	1.10	1.03	1.10	0.98	0.97	1.39	0.87	1.05	0.88	1.17	1.87	0.85
IC offshore	1.12	1.31	1.23	1.30	1.16	1.16	1.65	1.04	1.25	1.05	1.39	2.23	1.01
IIC offshore	1.04	1.22	1.14	1.21	1.08	1.08	1.53	0.96	1.16	0.97	1.29	2.07	0.94
IIIC offshore	0.93	1.09	1.02	1.09	0.97	0.97	1.37	0.87	1.04	0.87	1.15	1.86	0.84
IB offshore	1.13	1.31	1.23	1.31	1.17	1.16	1.65	1.04	1.26	1.05	1.39	2.24	1.01
IIB offshore	1.04	1.22	1.14	1.21	1.08	1.08	1.53	0.97	1.17	0.97	1.29	2.07	0.94
IIIB offshore	0.94	1.09	1.02	1.09	0.97	0.97	1.38	0.87	1.05	0.87	1.16	1.86	0.84
IA offshore	1.14	1.32	1.24	1.32	1.18	1.17	1.67	1.05	1.27	1.06	1.40	2.25	1.02
IIA offshore	1.05	1.23	1.15	1.22	1.09	1.09	1.54	0.97	1.17	0.98	1.30	2.09	0.94
IIIA offshore	0.94	1.10	1.03	1.10	0.98	0.97	1.38	0.87	1.05	0.88	1.16	1.87	0.85

Wind sites

Table 7: Life ratio $Lr_{IEC,WS}$

The results show that wind sites such as Moaleman and Aysha are categorized according to their annual mean wind speed as IEC III and II, respectively, but their bearing life is less than

that of related IECs. The results show that, although the contribution of overrated wind speed in Khaf is greater than that of IEC classes I and II, the IEC class II bearing has an acceptable life ratio. In addition, despite the high annual wind speed in Khaf, it is possible to use IEC Class II pitch bearings. The result of the life ratio of the Anholt offshore wind site compared to related IEC classes is close.

5. Conclusions

The wind speed distribution at offshore and onshore wind sites was studied. It is observed that, despite the fair performance of Rayleigh distribution in offshore wind sites, such distribution leads to greater uncertainty in wind distribution and load estimation in onshore sites. This is especially of interest since Rayleigh distribution is the preferred and most commonly used distribution in the wind turbine design standards. It is found that other distributions, for instance Kernel, perform well both in onshore and offshore wind sites, while using the Weibull distribution is also acceptable.

Furthermore, a calculation between the load and life of the pitch bearing and the wind speed is developed, and uncertainty in the loads based on the wind speed model is studied. The results illustrate the influence of wind speed on the pitch bearing loads and life. Pitch bearing life ratio results show that implementing IEC category-designed pitch bearings could result in an overestimate of bearing life compared to wind-site-designed pitch bearings. Moreover, pitch bearings with a lower IEC class design could tolerate the loads of wind sites with a higher annual wind speed.

Acknowledgement

The authors gratefully acknowledge the financial support of the Research Council of Norway through the InteDiag-WTCP project (Project Number 309205).

References

[1] J. Carta, P. Ramırez, and S. Velazquez. A review of wind speed probability distributions used in wind energy analysis. *Renewable and Sustainable Energy Reviews*, 13:933–955, 2009.

[2] O. Alavi, K. Mohammadi, and A. Mostafaeipour. Evaluating the suitability of wind speed probability distribution models: A case of study of east and southeast parts of iran. *Energy Conversion and Management*, 119:101–108, 2016.

[3] C. Jung and D. Schindler. Wind speed distribution selection – a review of recent development and progress. *Renewable and Sustainable Energy Reviews*, 119:109290, 2019.

[4] H. Shi, N. Xiao Z. Dong, and Q. Huang. Wind speed distributions used in wind energy assessment: A review. *Frontiers in Energy Research*, 9:769920, 2021.

[5] M. Ahsan ul Haq, S. Choudhary, A. AL-Marshadi, and M. Aslam. A new generalization of lindley distribution for modeling of wind speed data. *Energy Reports*, 8:1–11, 2022.

[6] GL. `GL-IV-1`: Guideline for the certification of wind turbines, 2010.

[7] IEC. `IEC`-61400-1: Wind energy generation system, part 1: Design requirements, 2019.

[8] E. K. Akpinar and S. Akpinar. A statistical analysis of wind speed data used in installation. *Energy Conversion and Management*, 46:515–532, 2005.

[9] T. P. Chang. Estimation of wind energy potential using different probability density functions. *Applied Energy*, 88:1848–1856, 2011.

[10] C. Dao, B. Kazemtabrizi, and C. Crabtree. Wind turbine reliability data review and impacts on levelised cost of energy. *Wind Energy*, 22(12):1848–1871, 2019.

[11] D. K. Andreasen, C. Rodenas-Soler, U. Oertel, K. Krügel, I. Reinares, I. S. Mendia, J. H. Nielsen, A. Olsen, A. Tinni, D. Vizireanu, J. Cheaytani, and P. Bousseau. WP2 Wind Turbine diagnosis/prognosis solution for a New Design. Physical D2.4 Portability of failure mode detection/prognosis orientations. Technical report, 2021.

[12] T. Harris, J.H. Rumbarger, and Butterfield C.P. Wind Turbine Design Guideline DG03: Yaw and Pitch Rolling Bearing Life. Technical report, NREL/TP-500-42362, National Renewable Energy Lab.(NREL), Golden, CO (United States), 2009.

[13] L. Wöll, G. Jacobs, and A. Kramer. Lifetime Calculation of Irregularly Oscillating Bearings in Offshore Winches. *Modeling, Identification and Control*, 39(2):61–72, 2018.

[14] G. Breslau and B. Schlecht. A fatigue life model for roller bearings in oscillatory applications. *Bearing World Journal*, 5:65–80, 2020.

[15] DNV. DNV-ST-0361, machinery for wind turbines, 2016.

[16] J. Yu, Y. Fu, Y. Yu, S. Wu, Y. Wu, M. You, S. Guo, and M. Li. Assessment of offshore wind characteristics and wind energy potential in bohai bay, china. *Energies*, 12(15), 2019.

[17] L. J. Bain and C. E. Antle. Estimation of parameters in the weibull distribution. *Technometrics*, 9:621–627, 1967.

[18] C. Dawson, R. Abrahart, and L. See. Hydrotest: a web-based toolbox of evaluation metrics for the standardised assessment of hydrological forecasts. *Environmental Modelling & Software*, 22(7):1034–1052, 2007.

[19] K. Mohammadi, O. Alavi, A. Mostafaeipour, N. Goudarzi, and M. Jalilvand. Assessing different parameters estimation methods of weibull distribution to compute wind power density. *Energy Conversion and Management*, 108:247–265, 2016.

[20] D. R. Legates and Gregory J. McCabe Jr. Evaluating the use of goodness-of-fit measures in hydrologic and hydroclimatic model validation. *WATER RESOURCES RESEARCH*, 35:233–241, 1999.

[21] C. G. Justus and A. Mikhail. Height variation of wind speed and wind distributions statistics. *Geophysical Research Letters*, 3:261–264, 1976.

[22] J. Jonkman, S. Butterfield, W. Musial, and G. Scott. Definition of a 5-MW reference wind turbine for offshore system development. Technical report, National Renewable Energy Lab.(NREL), Golden, CO (United States), 2009.

[23] NREL. Nrel 5mw reference turbine openfast model. `https://github.com/OpenFAST/r-test/tree/main/glue-codes/openfast/5MW_Baseline`, 2022. [Online; accessed 25-August-2022].

[24] A. Rezaei, Y. Guo, J. Keller, and A. R. Nejad. Effects of wind field characteristics on pitch bearing reliability: a case study of 5 mw reference wind turbine at onshore and offshore sites. *Forschung im Ingenieurwesen*, Under publication(-):1–18, 2023.

[25] NREL. Openfast. `https://github.com/OpenFAST/openfast`. [Online; accessed 2-August.-2022].

[26] J. Keller and Y. Guo. Rating of a pitch bearing for a 1.5-MW wind turbine. Technical report, NREL/TP-5000-82462, National Renewable Energy Lab.(NREL), Golden, CO (United States), 2022.

[27] O. Menck, M. Stammler, and F. Schleich. Fatigue lifetime calculation of wind turbine blade bearings considering blade-dependent load distribution. *Wind Energy Science*, 5(4):1743–1754, 2020.

[28] Renewable Energy and Energy Efficiency Organization (SATBA). `http://www.satba.gov.ir/en/`, 2022. [Online; accessed 24-May-2022].

[29] World Bank Group. Pakistan - wind measurement data. `https://energydata.info/dataset/pakistan-wind-measurement-data`, 2023. [Online; accessed 20-January-2023].

[30] GIZ. Vietnam - wind measurement data. `https://energydata.info/dataset/vietnam-wind-measurements-giz`, 2023. [Online; accessed 20-January-2023].

[31] World Bank Group. Ethiopia - wind measurement data. `https://energydata.info/dataset/ethiopia-wind-measurement-data`, 2023. [Online; accessed 20-January-2023].

[32] Ørsted. Green solutions: Offshore wind data. `https://orsted.com/en/our-business/offshore-wind/wind-data`, 2022. [Online; accessed 4-June-2022].

[33] D. Jager and A. Andreas. NREL National Wind Technology Center (NWTC): M2 Tower; Boulder, Colorado (Data);. Technical report, NREL Report No. DA-5500-56489, 1996.